Progress In Electromagnetics Research, Vol. 131, 185–194, 2012

INVESTIGATION OF BANDWIDTH ENHANCEMENT IN VOLUMETRIC LEFT-HANDED METAMATERIALS USING FRACTALS

T. M. De la Mata Luque, N. R. Devarapalli*, and C. G. Christodoulou

Department of Electrical and Computer Engineering, University of New Mexico, Albuquerque, NM 87131, USA

Abstract—Volumetric left-handed metamaterials made up of an array of split-ring resonators (SRRs) and wires exhibit negative index of refraction in a very narrow bandwidth due to the resonant nature of SRRs. We investigate the possible bandwidth enhancement by adding resonances to the system using fractals. The operating bandwidth of the system is increased when the additional resonances are placed close enough to each other. The Sierpiński-carpet fractal pattern is chosen as the distribution for the SRRs. The principle is demonstrated through simulations, and prototypes are fabricated and tested to verify consistency with simulations.

1. INTRODUCTION

A volumetric left-handed metamaterial (LHM) exhibiting negative index of refraction at microwave frequencies is considered; it consists of arrays of wires and split-ring resonators (SRRs) [1, 2]. Wires and their variants provide negative permittivity over broad bandwidths that lie below their plasma frequencies [3]. However, SRRs and their variants provide negative permeability over narrow bandwidths due to their resonant nature [4]. Consequently, simultaneous negative permittivity and permeability for an LHM occurs in a narrow bandwidth (BW) dictated by the SRRs.

SRRs and RLC circuits exhibit similarities [5, 6]. An SRR is made of a ring that can be modeled as an inductor, and a split as a capacitor; the losses are modeled as a resistor. The incident and transmitted electric/magnetic fields for SRRs play the role of input and

Received 16 July 2012, Accepted 29 August 2012, Scheduled 9 September 2012
* Corresponding author: Naga Ravi Kanth Devarapalli (nrdevara@gmail.com).

output voltages/currents in RLC circuits. Resonance characteristics of SRRs and RLC circuits are similar; losses are generally low and SRRs produce sharp resonances resulting in a narrow BW for LHMs.

2. SRR FRACTAL PATTERNS

To significantly alter the resonance frequency of an array of identical and uniformly distributed SRRs, either the individual dimensions of the SRRs or their spatial periodicity is modified [7–9]. We introduce SRRs of different sizes, analogous to adding parallel RLC branches to the original RLC circuit, to obtain new resonances in the system. When these resonances are designed to be close enough to each other, a wider BW is achieved.

SRRs of different sizes are introduced according to the Sierpiński-carpet fractal pattern (SFP). A unit cell of LHM consists of a unit cell of SRR(s) disposed according to the chosen fractal pattern on one face of the substrate and wires on the other face, as shown in Figure 1. Each of these unit cells repeats itself in the same manner (fixed periodicity) to obtain a different LHM. In Figure 1(a) (1(b)), the SRR(s) are disposed according to the first (second) order SFP. Higher order SFPs are also obtained in a similar manner. First order SFP

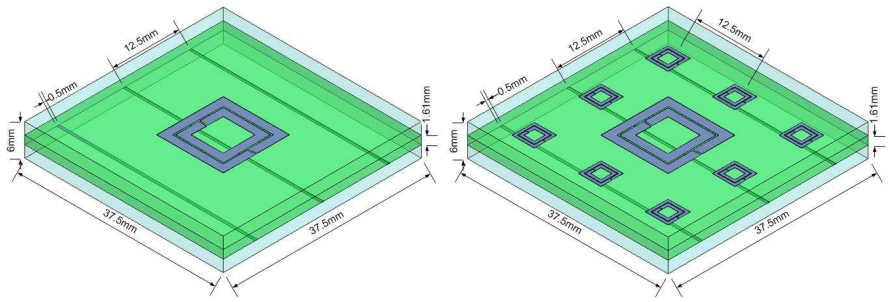

		l' (mm)	w (mm)	g (mm)
Structure-1	Large SRR	12.5	1.5	0.25
Structure-2	Large SRR	12.5	1.5	0.25
	Small SRR	4.17	0.5	0.1
Structure-3	Large SRR	12.5	1.5	0.8
	Small SRR	4.17	0.5	0.075

(c)

Figure 1. (a) Structure-1. (b) Structure-2. (c) SRR dimensions.

only has first order sub-squares; second order SFP has both first and second order sub-squares, and so on.

A unit cell with one SRR achieves a single resonance, and a unit cell with SRRs of different sizes achieves multiple resonances for an LHM. SRRs of different sizes produce different resonances, and the order of the SFP gives the number of resonances in the system. Theoretically, an infinite number of sizes of SRRs can be placed within one unit cell. However, the intensity of transmission at the different resonances obtained from the SFP is different. Notice that for the second and higher order sub-squares, there is a disorder in their periodicity. Moreover, the disorder intensifies with increasing order of sub-squares. The disorder in periodicity of higher order sub-squares is caused due to the presence of lower order sub-squares. The presence of this type of disorder contributes to reduction in the intensity of transmission at the resonant frequencies associated with the disordered sub-squares [11–13]. The intensity of transmission at a resonance associated with SRRs of a certain size is inversely proportional to their order. Through simulations it was observed that increasing the order of the SFP beyond three is not advisable as the intensity of transmission at the corresponding resonances reduces by 10 dB or more compared to that of the first order. LHMs obtained from the first and second order SFPs are presented in this work.

3. SIMULATIONS

Simulations are performed using the commercial software, HFSS. An LHM is simulated in HFSS as follows: a unit cell of LHM is placed inside a box of air surrounded by two pairs of master/slave (linked) or periodic boundary conditions along directions perpendicular to the wave propagation direction, and two one-mode Floquet ports along the wave propagation direction to measure S-parameters. A unit cell of LHM with the aforementioned periodic boundary conditions simulates the behavior of an LHM that extends to infinity along directions transverse to the wave propagation direction. Furthermore, the wires and SRR(s) in a unit cell of LHM are defined as electrically-perfect conducting surfaces with no thickness (due to limited computational capacity).

3.1. Fractal LHMs

Three LHM designs are presented. Structure-1 (Structure-2), shown in Figure 1(a) (Figure 1(b)), follows the first (second) order SFP and has one (two) resonance(s). Structure-2 and structure-3 differ only in one

dimension (g) of the SRRs, as labeled in Figure 1(c). The dimensions of the SRRs of the three structures are shown in the table adjacent to Figure 1(c).

The simulation results for structure-1 and structure-2 are shown along with their corresponding experimental results in Figure 6. For structure-1, the pass band is centered at approximately 4.87 GHz with a −3 dB BW of 80 MHz. For structure-2, two main resonances are found, one at 4.84 GHz with a −3 dB BW of 60 MHz, and the other at 6.10 GHz with a −3 dB BW of 40 MHz. The SFP of structure-2 slightly disturbs the desired periodicities in the structure, thereby creating other (weaker) resonances.

Structure-3 looks similar to structure-2; however it operates with the two dominant resonances brought close to each other in frequency. Figure 2 shows the simulation results for structure-3, where both the main resonances are now located at about 5.25 GHz; the resultant −3 dB BW is 120 MHz, a 50% increase when compared to that of structure-1.

3.2. Reconfigurable SRRs

The capability to instantaneously change the resonant frequency of an LHM through reconfigurable SRRs is desirable, and more so when used in conjunction with fractals. Placing additional splits in the SRRs' rings shifts their resonant frequency [7, 8, 10]. Additional splits are introduced in the SRRs' rings, as shown in Figure 3(a). Simulations

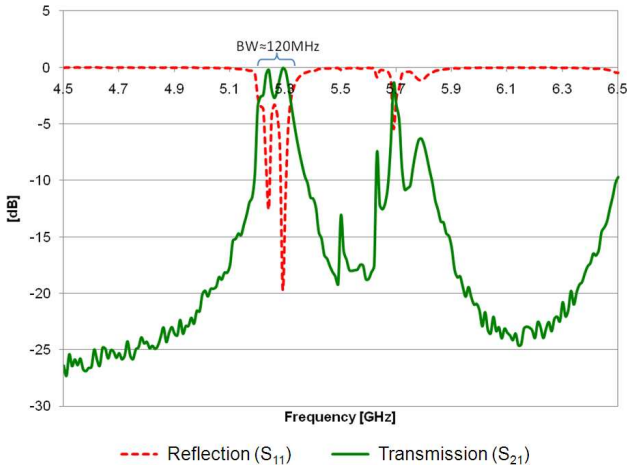

Figure 2. Simulation results for structure-3.

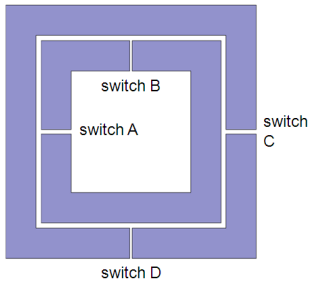

				Large SRRs	Small SRRs
A	B	C	D	Resonance (GHz)	Resonance (GHz)
0	0	0	0	6.31	7.72
0	0	0	1	5.7	5.96
0	0	1	0	5.5	5.94
0	1	0	0	5.45	6.98
0	1	0	1	5.03	5.46
0	1	1	0	4.15	6.35
1	0	0	0	5.11	6.9
1	0	0	1	4.08	5.31
1	0	1	0	4.63	5.72

(a)

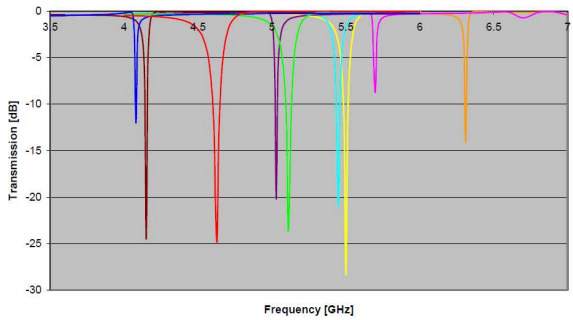

(b)

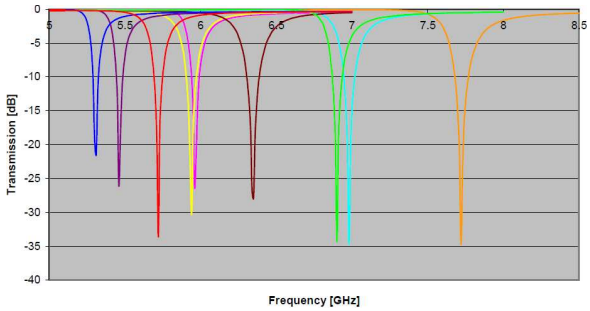

(c)

Figure 3. (a) Reconfigurable SRR. (b) Resonances for reconfigurable large SRRs. (c) Resonances for reconfigurable small SRRs.

are performed with various combinations of splits in closed (1)/open (0) conditions; the associated resonant frequencies for the SRRs are shown in the table adjacent to Figure 3(a).

Switches A (B) and C (D) for the large SRRs are said to be open when a split with $g = 2.5\,\text{mm}$ ($g = 0.12\,\text{mm}$) is maintained. A total of sixteen different combinations exist. However, seven out of the sixteen configurations do not have at least one split in each ring, and therefore

do not result in a magnetic resonance for the SRR. The remaining nine possible resonances range from 4.08 GHz to 6.31 GHz. The depth of resonance varies between −28 dB and −8 dB (as shown in Figure 3(b)) with an average value of approximately −20 dB. Switches A (B) and C (D) for the small SRRs are said to be open when a split with $g = 0.1$ mm ($g = 0.05$ mm) is maintained. The nine resonances for the small SRRs range from 5.31 GHz to 7.72 GHz, with intensity varying between −34.7 dB and −21.5 dB (as shown in Figure 3(c)). Notice that the resonances for the small and large SRRs have overlapping frequency ranges. Further optimizing this overlap allows the use of reconfigurable SRRs disposed according to a fractal pattern to obtain improved BW for all possible configurations in the enhanced operating frequency range of the LHM. Therefore there is scope for further investigation on the use of reconfigurable SRRs in the above stated manner.

4. EXPERIMENTS

To check the credibility of the results from simulations, two prototypes corresponding to structure-1 and structure-2 are manufactured; the corresponding simulations' results are experimentally verified. The prototype corresponding to structure-1 is referred to as prototype-1, shown in Figure 4(a), and the one corresponding to structure-2 as prototype-2, shown in Figure 4(b). A 1.61 mm thick Taconic® TLY-5A double-sided substrate with a relative dielectric constant of 2.17±0.02 and copper thickness of about 35 µm makes a printed circuit board (PCB) slab. Each of the prototype LHMs is built by interleaving PCB slabs and foam slabs. SRRs on one face of a PCB slab and wires on the other are mechanically processed using a milling machine. Foam slabs are used to simulate air. Finally, all the PCB slabs of a prototype are carefully aligned with the foam slabs interleaving them and the whole structure is clamped and set-up for measurements. LPKF ProtoMat® S62 milling machine delivering a resolution of up to 0.25 µm is used for mechanical processing. Six pieces of substrate and five pieces of

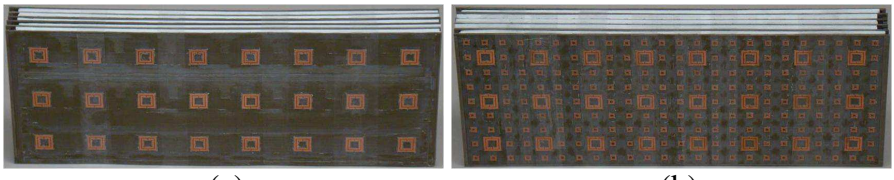

Figure 4. (a) Prototype-1. (b) Prototype-2.

foam are cut for each prototype. Each slab is 300 mm×112.5 mm and contains twenty four unit cells. Each prototype contains one hundred forty four unit cells: three unit cells in height, six unit cells in width and eight unit cells in length (along the direction of propagation). The arrangement of wires is identical for both prototypes and is shown in Figure 5(a) with respect to the SRRs of prototype-1.

Measurements are carried out inside an anechoic chamber to minimize interference. Figure 5(b) shows the experimental setup. The uniform plane wave required to illuminate each of the LHMs is approximately generated at the location of the LHM using a pyramidal horn antenna operating in the TE_{10} mode with lowest recommended operating frequency of 3.95 GHz, which is less than the lowest resonance of the LHMs: 4.84 GHz. Each LHM is placed approximately 1.7 m from the transmitter, which is in the horn's far-field for all radiating frequencies. Each LHM is aligned to be symmetric about the central-axis, which is along the length of the LHM and also along the aperture-normal at the center of the horn's aperture. The receiver is an open waveguide. Each LHM is placed such that all the fields entering the receiver pass through the LHM. Non-conductive pedestals are used to support the transmitter/receiver to minimize interference.

Agilent 8510C vector network analyzer is used to measure the transmission (S_{21}) parameter. The measured/simulated transmission coefficient corresponding to prototype-1/structure-1 (prototype-2/structure-2) is shown in Figure 6(a) (Figure 6(b)). For prototype-1, the measured peak transmission is found to be centered around 4.8375 GHz. Measurements on prototype-2 reveal two dominant transmission peaks as expected: one centered around 4.785 GHz and the

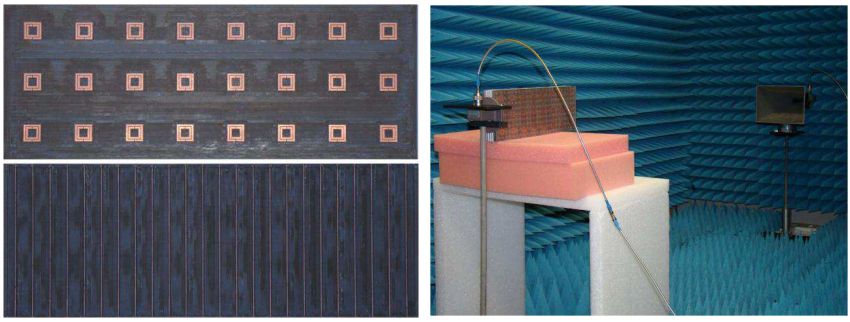

Figure 5. (a) Arrangement of wires with respect to SRRs for prototype-1. (b) Experimental set-up for measuring transmission.

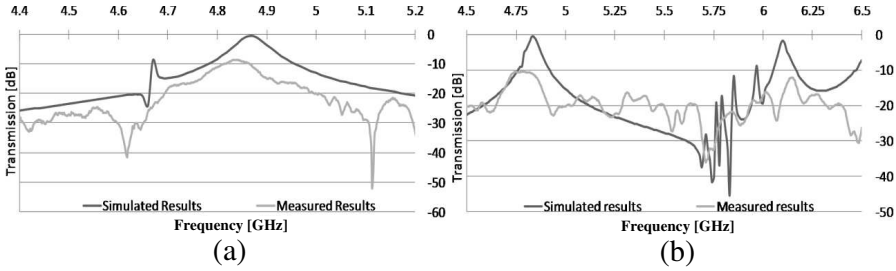

Figure 6. (a) Measured/simulated transmission coefficient for prototype-1/structure-1. (b) Measured/simulated transmission coefficient for prototype-2/structure-2.

other around 6.145 GHz. The locations of the dominant transmission peaks in frequency agree well with simulations.

Some parameters in which discrepancies appear between the results from simulations and experiments are: transmission level at dominant peaks, the number of weaker resonances, and the BWs associated with the dominant resonances. However, experiments do demonstrate that the locations of dominant resonant peaks in frequency are predictable with an accuracy of about 99%. The discrepancies are explained as follows.

The most evident difference between the results from simulations and experiments is the transmission loss at the dominant resonances, and it is more significant in the experimental results. In simulations, perfect electric conductors are used for wires/SRRs, and air separated the PCB slabs. However, foam is used instead of air and wires/SRRs are made from copper in experiments. For better correlation between simulation and experimental results, real metallic sheets with a prescribed thickness should be modeled in the simulations. However, due to limited computational capacity, electrically-perfect conducting surfaces with no thickness (electrically-perfect conducting boundaries) are used in simulations. Simulations utilize a single unit cell along with periodic boundary conditions to avoid edge-effects. However, due to finite extent of the prototypes in experiments there is power loss from diffraction/scattering at their edges. Power loss is also present due to burrs around wires/SRRs from machining imperfections. Machining imperfections also cause additional transmission peaks in experiments, although they are at least 5 dB below the dominant resonances. For instance, a few slightly wider splits in SRRs' rings cause resonances at higher frequencies [7]; in turn, the dominant resonance is also weakened. There is also discrepancy in the dominant resonance-BWs. Simulations use only a one-unit-cell-thick LHM along the direction of

propagation due to computational limitations. However, experiments utilize an eight-unit-cell-thick LHM, and coupling among SRRs along the direction of propagation improves BW [10, 14, 15].

5. CONCLUSIONS

The overall response of each fabricated LHM is consistent with simulations. Peaks of transmission occur at the design frequencies with about 99% accuracy and bandwidth enhancement is observed in volumetric left-handed metamaterials by introducing the Sierpiński-carpet fractal pattern. The possibility of designing reconfigurable LHMs for further improvement in the range of operating frequencies is also briefly discussed.

REFERENCES

1. Smith, D. R., W. J. Padilla, D. C. Vier, S. C. Nemat-Nasser, and S. Schultz, "Composite medium with simultaneously negative permeability and permittivity," *Phys. Rev. Lett.*, Vol. 84, No. 18, 4184–4187, May 2000.
2. Shelby, R. A., D. R. Smith, and S. Schultz, "Experimental verification of a negative index of refraction," *Science*, Vol. 292, No. 5514, 77–79, Feb. 2001.
3. Pendry, J. B., "Extremely low frequency plasmons in metallic mesostructures," *Phys. Rev. Lett.*, Vol. 76, No. 25, 4773–4776, Jun. 1996.
4. Pendry, J. B., A. J. Holden, D. J. Robbins, and W. J. Stewart, "Magnetism from conductors and enhanced nonlinear phenomena," *IEEE Trans. Microwave Theory Tech.*, Vol. 47, No. 11, 2075–2084, Nov. 1999.
5. Wu, Q., M. Wu, F. Meng, J. Wu, and L. Li, "Modeling the effects of an individual SRR by equivalent circuit method," *IEEE AP-S Int. Symp. Dig.*, 631–634, Jul. 2005.
6. Yasar-Orten, P., E. Ekmekci, and G. Turhan-Sayan, "Equivalent circuit models for split-ring resonator arrays," *PIERS Proceedings*, 534–537, Cambridge, USA, Jul. 5–8, 2010.
7. Aydin, K., I. Bulu, K. Guven, M. Kafesaki, C. M. Soukoulis, and E. Ozbay, "Investigation of magnetic resonances for different split-ring resonator parameters and designs," *New J. Phys.*, Vol. 7, No. 168, 1–15, Aug. 2005.
8. Chen, J.-Y., W.-L. Chen, J.-Y. Yeh, L.-W. Chen, and C.-C. Wang, "Comparative analysis of split-ring resonators for

tunable negative permeability metamaterials based on anisotropic dielectric substrates," *Progress In Electromagnetics Research M*, Vol. 10, 25–38, 2009.

9. Scheuer, J., "Ultra-high enhancement of the field concentration in split ring resonators by azimuthally polarized excitation," *Opt. Express*, Vol. 19, No. 25, 25454–25464, Dec. 2011.
10. Penciu, R. S., K. Aydin, M. Kafesaki, T. Koschny, E. Ozbay, E. N. Economou, and C. M. Soukoulis, "Multi-gap individual and coupled split-ring resonator structures," *Opt. Express*, Vol. 16, No. 22, 18131–18144, Oct. 2008.
11. Aydin, K. and E. Ozbay, "Experimental investigation of reflection characteristics of left-handed metamaterials in free space," *IET Microw. Antennas Propag.*, Vol. 1, No. 1, 89–93, Feb. 2007.
12. Papasimakis, N., V. A. Fedotov, Y. H. Fu, D. P. Tsai, and N. I. Zheludev, "Coherent and incoherent metamaterials and order-disorder transitions," *Phys. Rev. B*, Vol. 80, 041102, 2009.
13. Aydin, K. and K. Guven, "Effect of disorder on magnetic resonance band gap of split-ring resonator structures," *Opt. Express*, Vol. 12, No. 24, 5896–5901, Nov. 2004.
14. Gay-Balmaz, P. and O. Martin, "Electromagnetic resonances in individual and coupled slit-ring resonators," *J. Appl. Phys.*, Vol. 92, No. 5, 2929–2936, Sep. 2002.
15. Carbonell, J., E. Lheurette, and D. Lippens, "From rejection to transmission with stacked arrays of split ring resonators," *Progress In Electromagnetics Research*, Vol. 112, 215–224, 2011.